NEW METHODS FOR WIDE-BASELINE IMAGE INTERPOLATION

by

JEFF WOOD

Presented to the Faculty of the Graduate School of
The University of Texas at Arlington in Partial Fulfillment
of the Requirements
for the Degree of

MASTER OF SCIENCE

THE UNIVERSITY OF TEXAS AT ARLINGTON
December 2016

Copyright © by Jeff Wood 2016

All Rights Reserved

To my mother Sari and my uncle Luis Alfredo (my father figure)

who set the example and who made me who I am.

ACKNOWLEDGEMENTS

I would like to thank my supervising professor Dr. Vasant Prabhu for constantly motivating and encouraging me, and also for his invaluable advice during the course of my doctoral studies. I wish to thank my academic advisors Dr. Jonathan Bredow, Dr. Chien-Pai Han, Dr. Harold Sobol, Dr. Saibun Tjuatja and Dr. Stone Tseng for their interest in my research and for taking time to serve in my dissertation committee.

I would also like to extend my appreciation to Nortel Networks for providing financial support for my doctoral studies. I wish to thank Meng Yee, Robert Hunt and Dr. Michael Maragoudakis with Wireless Network Engineering for their support and encouragement. I am especially grateful to Mazin Al-Shalash for his interest in my research and for the helpful discussions and invaluable comments. I wish also to thank Dr. Yaser Ibrahim, Dr. Mini Vassudevan and Kal Mustafa for taking the time to critically evaluate this manuscript.

I am grateful to all the teachers who taught me during the years I spent in school, first in Palestine, then in Iraq and finally in the Unites States. I would like to thank Dr. Saleh Al-Araji for encouraging and inspiring me to pursue graduate studies.

Finally, I would like to express my deep gratitude to my brothers who have encouraged and inspired me and sponsored my undergraduate and graduate studies. I am extremely fortunate to be so blessed. I am also extremely grateful to my mother,

sister and wife for their sacrifice, encouragement and patience. I also thank several of my friends who have helped me throughout my career.

November 15, 2003

ABSTRACT

NEW METHODS FOR WIDE-BASELINE
IMAGE INTERPOLATION

Jeff Wood, M.S.

The University of Texas at Arlington, 2016

Supervising Professor: Farhad Kamangar

The increasing demand for voice and data capacity has been the primary motivation for cellular and PCS evolution. Cohere detection is the most power-efficient scheme that is capable of providing substantial improvement in system capacity over noncoherent and differentially coherent schemes. For this reason, reverse link coherent detection is being considered as the framework for third generation wireless communication systems. In mobile communications, however. rapid fading may preclude a good estimate of the channel phase required to achieve coherent demodulation. This may lead to serious degradation to system performance. This dissertation investigates the capacity and error-rate performance of coherent systems with imperfect carrier recovery. These systems are known as partially coherent systems.

Partially coherent systems have not received thorough investigation in the literature. Most of the previous work has been focused on the analysis of performance for BPSK over AWGN channels. Upper bounds on bit error probability have been derived, but found to be very conservative for the range of carrier phase jitter vari-

ance of practical interest. The error performance for partially coherent QPSK has not received much attention. Furthermore, the performance of partially coherent systems over multipath fading channels with diversity has not been studied.

In this dissertation, several upper and lower bounds on the error performance of partially coherent systems are derived by the application of Jensen's inequality and the isomorphism theorem from the theory of moment spaces assuming that the carrier phase error could have either Tikhonov or Gaussian distribution. An analytical method based on Gram-Charlier series expansion is also developed for the computation of the error probability and signal-to-noise ratio distribution of partially coherent systems over fading channels with diversity.

The application of partially cohere systems for CDMA mobile cellular communication is also investigated. performance impairments due to thermal noise, multipath fading, multiple access interference and self-noise are included in the analysis. A design criterion for adding weak signals with equal gain combining is established when the multipath intensity profile is nonuniform.

TABLE OF CONTENTS

LIST OF ILLUSTRATIONS

LIST OF TABLES

COMMONLY USED SYMBOLS AND NOTATION

Symbol	Description
$\mathbf{v}$	*Vectors* in *lowercase* bold
v_a	a-component of vector $\mathbf{v}$
$\mathbf{M}$	*Matrices* in *uppercase* bold
$M_{r,c}$	Entry in row r and column c of matrix $\mathbf{M}$
$\mathbf{m}_c$	*Vector* occurring in column c of matrix $\mathbf{M}$
$\mathbf{x}$	Generic 3-dimensional spatial coordinate
$\tilde{\mathbf{x}}$	Generic 3-dimensional spatial coordinate (expressed *homogeneously*)
$\mathbf{y}$	Generic 2-dimensionals image coordinate
$\tilde{\mathbf{y}}$	Generic 2-dimensional image coordinate (expressed *homogeneously*)
$\mathbf{u}$	Pixelized 2-dimensional image coordinate
$\tilde{\mathbf{u}}$	Pixelized 2-dimensional image coordinate (expressed *homogeneously*)
${}^{A}\mathbf{x}$	Generic 3-dimensional spatial coordinate in reference frame A
${}^{A}\tilde{\mathbf{x}}$	Generic 3-dimensional spatial coordinate (expressed *homogeneously*) in reference frame A
${}^{C}_{B}\tilde{\mathbf{M}}$	Change from of reference frame B to reference frame C
s	Normalizing factor applied to *homogeneous* vector $\tilde{\mathbf{v}}$ such that original $\mathbf{v} = s \cdot \tilde{\mathbf{v}}$ is recovered

${}^{D}\mathbb{S}$	Spatial reference frame D
$[\mathbf{x}]_{\times}$	Skew-symmetric matrix version of vector $\mathbf{x}$ used as *left*-operand in the *cross*-product such that $[\mathbf{x}]_{\times} \cdot \mathbf{y} = \mathbf{x} \times \mathbf{y}$
l	Epipolar line
$\mathbb{P}$	Ray (or *pencil*) of all possible vectors $\mathbf{x}$ where $\mathbf{x} = s \cdot \tilde{\mathbf{x}}$ for some value of s

CHAPTER 1

Background

Oridinarily, real-world data contains 3-dimensions. Because standard images only include 2-dimensional data, information regarding depth is lost (i.e. it is often difficult to judge distance from a single image without visual cues). *Stereovision* attempts to resolved this by finding the same point in both *stereoscopic* images (known as a *corresponding point*), and recovering the depth information. An elementry example of this occurs in stereoscopic images with relatively low distance between cameras (i.e they are righht next to each other). Objects that are *farther* away from the observer occur closer together in the stereo images, whereas objects *closer* to the camera appear appear farther appart in the stereo-images.

1.1 Change of Reference

Each view from a pair of stereo-images encompasses its own *frame of reference* (i.e. the directions of *forward* or *backward* are unique to image and may differe considerably depending on camera displacement). This requires expressing points from different frames of reference (traditionally referred to *left* and *right*) in a single reference frame. As such it is necessary to be able to express coordinates in a given reference frame in any other reference frame.

Coordinates given in ${}^{A}\mathbf{x}$ can be expressed in ${}^{B}\mathbf{x}$ by the geometric transformation:

$$^{B}\mathbf{x} = {}^{B}_{A}\mathbf{R} \cdot {}^{A}\mathbf{x} + {}^{B}_{A}\mathbf{t}$$

or

$$^{B}\tilde{\mathbf{x}} = \left[\begin{array}{c|c} {}^{B}_{A}\mathbf{R} & {}^{B}_{A}\mathbf{t} \\ \hline 0 & 1 \end{array}\right] \cdot {}^{A}\tilde{\mathbf{x}}$$

$$= {}^{B}_{A}\mathbf{M} \cdot {}^{A}\tilde{\mathbf{x}}$$

where ${}^{B}_{A}\mathbf{M}$ is also the geometric transformation necessary to transform ${}^{B}\mathbb{S}$ into ${}^{A}\mathbb{S}$.

Withough calculating any new quantities, rearranging allows us to express coordinates in ${}^{B}\mathbf{x}$ in the ${}^{A}\mathbf{x}$ reference frame as:

$${}^{B}_{A}\mathbf{R}^{\intercal} \cdot ({}^{B}\mathbf{x} - {}^{B}_{A}\mathbf{t}) = {}^{A}\mathbf{x}$$

and similarly transforms ${}^{A}\mathbb{S}$ into ${}^{B}\mathbb{S}$.

1.2 Points and Lines in the Image Plane

Points in *world-space* of $\mathbb{R}^3$ are converted to points in the *image-plane* of $\mathbb{R}^2$ by *homogenization*. This occurs when a *world-coordinate* of $\mathbf{x} = [x_1, x_2, x_3]^{\intercal}$ is mapped to a *homogeneous image coordinate* of $\tilde{\mathbf{y}} = [y_1, y_2, 1]^{\intercal} = [x_1/x_3,\ x_2/x_3,\ x_3/x_3]^{\intercal}$ or a *non-homogeneous image coordinate* of $\mathbf{y} = [y_1, y_2]^{\intercal} = [x_1/x_3,\ x_2/x_3]^{\intercal}$. Points of the form $\tilde{\mathbf{y}} = [y_1, y_2, 0]^{\intercal}$ are special case of homogeneous point referred to as a *point at infinity*.

Lines in $\mathbb{R}^2$ can be represented in different contexts. The *vector offset* method calculates a line $\mathbf{s}(t)$ between points $\mathbf{y_1}$ and $\mathbf{y_2}$ as

$$\begin{aligned}\mathbf{s}(t) &= (1-t)\cdot\mathbf{y_1} + t\cdot\mathbf{y_2} \\ &= \mathbf{y_1} + t\cdot(\mathbf{y_2}-\mathbf{y_1})\end{aligned}$$

in which the line is parrallel to the vector $\mathbf{y_2}-\mathbf{y_1}$ and offset from the origin by the vector $\mathbf{y_1}$. Lines are also represented by their coefficients as $\mathbf{l} = [a, b, c]^\intercal$ where

$$\begin{aligned}\mathbf{l}^\intercal\cdot\tilde{\mathbf{y}} &= \begin{bmatrix} a & b & c \end{bmatrix}\cdot\begin{bmatrix} y_1 \\ y_2 \\ 1 \end{bmatrix} \\ &= a\cdot y_1 + b\cdot y_2 + c\cdot 1 \\ &= 0\end{aligned}$$

This definition lets us say $\tilde{\mathbf{y}}$ is located on line $\mathbf{l}$ *if and only if* $\mathbf{l}^\intercal\cdot\tilde{\mathbf{y}} = 0$. The line $\mathbf{l}$ joining two *homogeneous image coordinates* $\tilde{\mathbf{y}}_\mathbf{1}$ and $\tilde{\mathbf{y}}_\mathbf{2}$ is then calculated as the cross product of $\mathbf{l} = \tilde{\mathbf{y}}_\mathbf{1}\times\tilde{\mathbf{y}}_\mathbf{2}$.

1.3 Epipolar Geometry

Each point of of interest (also referred to as a *feature*) in a single image occurs in a 2-dimensional space at location $\tilde{\mathbf{y}} = [x, y, 1]^\intercal$. The same point in space when viewed from an image at a similar (though different) angle is referred to as a *corresponding*

point with location of $\tilde{\mathbf{y}}' = [x', y', 1]^\intercal$[1]. This set of infinitley many points form a 1-dimensional subspace (also known as a *pencil*) of the 3-dimensional world space.

The pencil, when viewed from an image at a different angled-position, appears as a line $\mathbf{l}' = [A', B', C']^\intercal$, known as the *epipolar line*. The fact that the corresponding point (in the *angled image*) of $\tilde{\mathbf{y}}' = [x', y', 1]^\intercal$ occurs on this epipolar line is referred to as the *epipolar constraint*. It is formalized, using the previously given *line-point equality* of $\mathbf{l}'^\intercal \cdot \tilde{\mathbf{y}}' = 0$ for the *angled* image. Similarly, the corresponding point of $\tilde{\mathbf{y}}' = [x', y', 1]^\intercal$ produces an epipolar line in the *original image* of $\mathbf{l} = [A, B, C]$. The original point of $\tilde{\mathbf{y}} = [x, y, 1]^\intercal$ must lie located on this epipolar line as required by the epipolar constraint, resulting in the *line-point equality* of $\mathbf{l}^\intercal \cdot \tilde{\mathbf{y}} = 0$ for the *original image*.

When viewed in ther respective images, each point ($\tilde{\mathbf{y}}$ and $\tilde{\mathbf{y}}'$) has a pencil that coincides with that point. Since the pencils act as *directional*-vectors in 3-dimensional space, there is a unique 2-dimensional plane which contain both of these vectors, known as the *epipolar plane*. It is the intersection of the epipolar plane with the *original image*-plane and the *angled image*-plane that results in the epipolar lines of $\mathbf{l}$ and $\mathbf{l}'$, respectively. In fact, the *epipolar plane* (in each image's *coordinate systems*)[2] has the same vector form as its epipolar line. Specifically, in the *original image* reference frame $\mathbf{l} = \mathbf{P} = [A, B, C]^\intercal$, and in the *angled image* reference frame $\mathbf{l}' = \mathbf{P}' = [A', B', C']^\intercal$. This results from the fact that any *world*-point $\mathbf{x}$ lying on the *epipolar plane* $\mathbf{P}$ will result in a *homogeneous image*-point $\tilde{\mathbf{y}}$ that also lies on the

[1] A *change of reference* is implied between cooridinates $\tilde{\mathbf{y}} = [x', y', 1]^\intercal$ and $\tilde{\mathbf{y}}' = [x', y', 1]^\intercal$. The majority of corresponding points do not occur at the same *image coordinates* between images (i.e $\tilde{\mathbf{y}} \neq \tilde{\mathbf{y}}'$. The only way a single *world coordinate* can yield different *image coordinates*, is if a *change of reference* occurs in *world space* each time the *image coordinates* are obtained by dividing by z_{world}.

[2] There is a single *epipolar plane* for each pair of corresponding points $\tilde{\mathbf{y}}$ and $\tilde{\mathbf{y}}'$. However, the single plane can be parameterized infinitley many ways, depending on the *frame of reference*

plane $\mathbf{P}$. Specifically, when $\mathbf{x} = s \cdot \tilde{\mathbf{y}}$ for some non-zero value of s, then $\mathbf{P}^\intercal \cdot \mathbf{x} = 0$ implies $\mathbf{P}^\intercal \cdot \mathbf{x} = \mathbf{P}^\intercal \cdot (s \cdot \tilde{\mathbf{y}}) = 0$. Since $s \neq 0$, its true that $\mathbf{P}^\intercal \cdot \tilde{\mathbf{y}} = 0$.

In the majority of images, the sets of epipolar lines will converge at a point known as an *epipole*, denoted as $\mathbf{e}$ in the *original image* $\mathbf{e}'$ in the *angled image*.

1.4 Fundamental Matrix

In stereo vision, points ($\tilde{\mathbf{x}}$) in one image I are related to the epipolar line (l') that contain the corresponding point ($\tilde{\mathbf{x}}'$) by the *Fundamental Matrix* ($\mathbf{F}$).

$$l' = \mathbf{F} \cdot \tilde{\mathbf{x}}$$

1.5 Intrinsic Calibration Matrix

A point $\mathbf{x}$ in the *camera-coordinate system* of $\mathbb{R}^3$ is projected to the point $\tilde{\mathbf{y}}$ in $\mathbb{R}^2$ by means of the *pinhole camera model*. The set of all $\tilde{\mathbf{y}}$ are the result of *rays* passing through the *image plane* located at $z = f$, and converging at the *optical center* as shown in the figure below:
The location of $\tilde{\mathbf{y}}$ is determined by utilizing the *similarity of triangles* between $\mathbf{x}$ and $\tilde{\mathbf{y}}$. Specifically, we see that $y_1/f = x_1/x_3$ and $y_2/f = x_2/x_3$ lets us exprss the *image coordinate* $\tilde{\mathbf{y}}$ as $y_1 = f \cdot x_1/x_3$ and $y_2 = f \cdot x_2/x_3$. The point in the *image plane* of $\tilde{\mathbf{y}}$ is derived from the point $\mathbf{x}$ in *camera space* by means of the the *Camera Projection Matrix* $\mathbf{P}$ such that

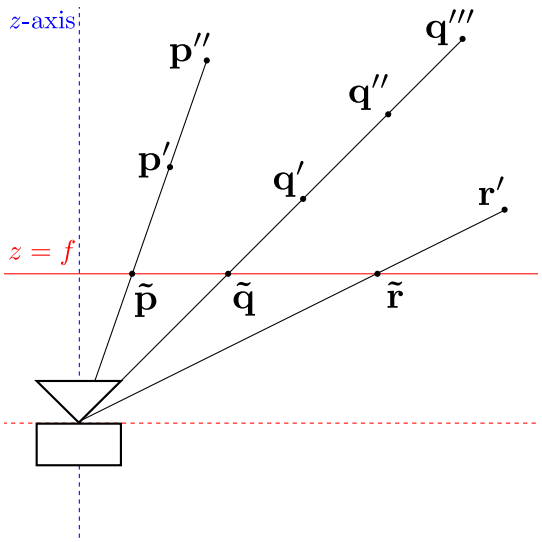

Figure 1.1. Pinhole CameraModel.

$$\mathbf{P}\cdot\tilde{\mathbf{x}} = \begin{bmatrix} f & 0 & 0 & 0 \\ 0 & f & 0 & 0 \\ 0 & 0 & 1 & 0 \end{bmatrix} \begin{bmatrix} x_1 \\ x_2 \\ x_3 \\ 1 \end{bmatrix} = \begin{bmatrix} f\cdot x_1 \\ f\cdot x_2 \\ x_3 \end{bmatrix}$$

$$= x_3 \cdot \begin{bmatrix} f\cdot x_1/x_3 \\ f\cdot x_2/x_3 \\ 1 \end{bmatrix} = x_3\cdot\tilde{\mathbf{y}}$$

This results in points $\tilde{\mathbf{x}}$ containing infinitley large values of x_3 being mapped to the same point $\tilde{\mathbf{y}}$ in the *image plane*. This point $\mathbf{y} = 0$ is referred to as the *principal point* in the *image plane*. This assumes the *principal point* is always located in the *image plane* at $\mathbf{y} = 0$. Projecting point $\tilde{\mathbf{x}}$ to the *image plane* with arbi-

trary *principal point* $\mathbf{p} = [p_x, p_y]^\intercal$ requires modifying the *projection matrix* to include *camera-specific* parameters. The *camera calibration matrix* $\mathbf{K}$ is given as

$$\mathbf{P} \cdot \tilde{\mathbf{x}} = \begin{bmatrix} f & 0 & p_x & 0 \\ 0 & f & p_y & 0 \\ 0 & 0 & 1 & 0 \end{bmatrix} \begin{bmatrix} x_1 \\ x_2 \\ x_3 \\ 1 \end{bmatrix} = \begin{bmatrix} f \cdot x_1 + p_x \cdot x_3 \\ f \cdot x_2 + p_y \cdot x_3 \\ x_3 \end{bmatrix}$$

$$= x_3 \cdot \begin{bmatrix} f \cdot x_1 / x_3 + p_x \\ f \cdot x_2 / x_3 + p_y \\ 1 \end{bmatrix} = x_3 \cdot \tilde{\mathbf{y}}$$

1.6 Essential Matrix

When coordinates from a reference frame are expressed as *normalized image coordinates* the range of possible NIC values in the corresponding image are given by the

CHAPTER 2

INTRODUCTION

2.1 Common formatting problems when using LaTeX to write the dissertation.

1. The most common formatting problem is that the bottom margin of all pages is not between 1.25 and 1.5 inches. The left and right margins are not between 1.25 and 1.5 inches. This is true regardless of whether you are using LaTeX on Linux or Windows.

   Solution: The problem with this is that dvipdf defaults to a paper size of A4, which is longer and narrower than 8.5" by 11". This affects the left, right, and bottom margins. To produce a document with the correct dimensions, in Linux first generate the DVI file. Convert this file to postscript, then convert the postscript file to PDF using the following two commands:

   ```
   dvips -t letter -Ppdf -G0 utaexample.dvi
   ps2pdf utaexample.ps
   ```

   If you are using LaTeX on Windows, you may (depending on how your environment is configured) be able to open a command window and type

   ```
   dvips -t letter -Ppdf -G0 utaexample.dvi
   ps2pdf utaexample.ps
   ```

   to generate a PDF with the correct dimensions.

2. Titles in the front matter and text longer than one line are appearing double-spaced in the front matter, but they should be single spaced.

   Solution: The sample document included with the template show examples of this and how to correct them. Basically, at the point where you have the section

title, caption title, etc., you need to create two versions of it. One version will appear at that location in the document, the other version will appear in the table of contents and will include formatting commands specifically for the table of contents. YOU DO NOT HAVE TO CHANGE THE TEMPLATE ITSELF FOR THIS PROBLEM.

2.2 Introduction

Mobile station (MS) needs to maintain a target E_b/N_0 in a power-controlled CDMA system to achieve the required frame error rate. The fraction of base station (BS) power required by the MS to maintain the target E_b/N_0 is different when the MS is in different operation mode. When the MS is connected to multiple BSs, it is said to be in soft handoff mode (SHM). While the MS is only connected to a single BS, it is said to be in non-soft handoff mode (NSHM). The MS in SHM achieves the macrodiversity gain and decreases the power required from the base stations that it is connected to. Current literature usually models E_b/N_0 as a random variable to calculate outage probability and capacity [1]. However, the E_b/N_0 is actually a constant value (or a small range of value) from the power-control viewpoint. When E_b/N_0 at the MS is less than the target value, the MS asks BSs to increase the transmitted power. When the fraction of BS power required by MS exceeds the maximum threshold, MS would not be able to maintain target E_b/N_0, which could lead to the dropout of the connections. Therefore, it is more appropriate to evaluate the system performance from the viewpoint of the fraction of BS power allocated to the MS.

Different approaches exist in the literatures to classify the MS to be in SHM or NSHM. Lee and Steel [1] proposed the concept of soft handoff zone (SHZ) and non-soft handoff zone (NSHZ). The NSHZ is the area around the reference BS within

radius less than a certain distance R_h. The MS in NSHZ is only connected to the reference BS regardless of the signal strengths received from other BSs. The SHZ is the area around the reference BS with radius greater than R_h but less than the cell radius R. The MS in SHZ utilizes all the received signals from the surrounding BSs. The location of the boundary of SHZ and NSHZ is determined by the pilot strength between two BSs and the shadowing effect is ignored. R_h is chosen to be $0.84R$. This approach was adopted in a large number of literatures [1] . By putting the MS in SHZ and NSHZ, the problem of soft handoff becomes simpler. However, there are unconvincing disadvantages of the above approach. First, explicit classification of SHZ and NSHZ does not exist in practical CDMA systems. As the MS in SHZ can still maintain the target E_b/N_0 by only connected to the reference BS and vice versa. Second, the R_h can not be explicitly defined by only the path loss without considering the shadowing effects. As shadowing fading exists, the MS in NSHZ may need to connect to multiple BSs to maintain the target E_b/N_0 and vice versa. Therefore, it is more accurate to define SH and NSH by considering the path loss including the shadowing effect and considering NSH for the MS in SHZ and SH for the MS in NSHZ. In this paper, we propose to use the relative soft handoff threshold to classify the MSs in SHM and NSHM. Using this approach, the BSs that the MS is connected to is determined by the path loss difference from that of a reference BS, where the reference BS has the lowest path loss (or the strongest signal). The path loss difference is the soft handoff threshold (SHT). Using that model, the MS in the SHZ can be in SH with other BSs with a certain probability.

Using the proposed soft handoff model and assuming the Rake receiver at the MS use channel-gain-and-interference matched approach to combine the recevied signals from different BSs . We further simplify the expression of E_b/N_0 into one term and derive the probability density function (PDF) of the fraction of BS power al-

locted to the MS. By imposing an upper limit on the maximum fraction of BS power (MFBP) allocated to the MS, the capacity and outgage probability is derived analytically. We show that the location of SH boundary, which is defiend at the limitation of the system capacity, is determined by the MFBP and SHT. We further show that contradict to what commonly believed in previous literatures, the SH can provide capacity gain only at a larger MFBP and SHT. SH in this case only has the advantage of reducing the outage probability.

This paper is organized as follows. Section II discusses the system model and how to use path loss with shadowing and relative soft handoff threshold to classify the MS in SHM or NSHM. Section III shows the derivation of the distribution of the BS power. The analytical derivation of the capacity and outage probability are also presented in this section. Section IV gives the numerical results and shows how the MFBP and SHT affect capacity and outage. Section V summarizes the results.

2.3 System model

In our analysis, a 13 cells cluster is considered and shown in Fig. 2.1 in order to minimize edge effect, which is caused if the BSs surrounding the MS is not symmetric. Only MSs inside the triangle shown in Fig. 2.1 are considered. Due to the symmetry in the structure, the performance matrix of the system obtained in this triangle can be generalized to the whole reference cell.

2.3.1 Soft Handoff Model

The SH approach used in the industry is complex to analyze.

For example, IS-95 uses fixed or constant T_{ADD}, T_{DROP} handoff thresholds and a T_{TDROP} timer to choose the BSs in the active set, which is defined as the set of BSs that the MS is communicating with and requiring power from. When the estimated

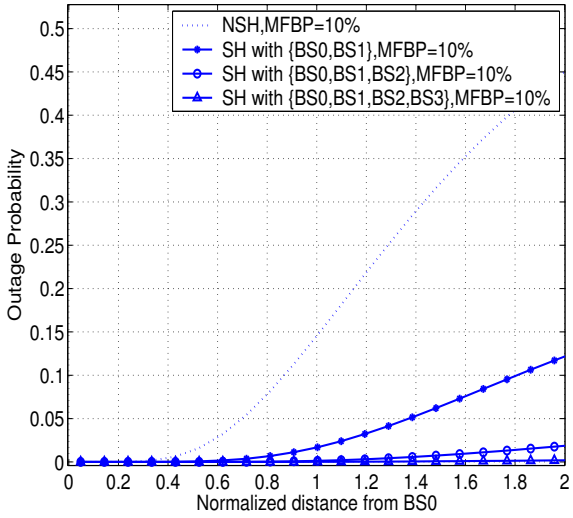

Figure 2.1. Cell structure.

Table 2.1. Base Class 0 System Frequecies

System	Reverse Link (MHz)	Forward Link (MHz)
A	824-835	869-880
	845-846.5	890-891.5
B	835-845	880-890
	846.5-849	891.5-894

pilot signal strength from a certain BS is above T_{ADD}, that BS is put into the active set. The MS combines signals from up to two BSs in the active set and having stronger pilot strengths. If pilot signal strength BSs in active sets drops below T_{DROP} for at least T_{TDROP} time, the BS is taken away from the active set [1]. The signal strength in IS-95 is defined as the energy-per-chip-to-interference ratio of the pilot channel. However, we can define pilot signal strength as the inverse of path loss with shadowing to effectively classify the MS into NSHM and SHM for the following reasons: First, the active set should be designed to be as stable as possible, which means the fast

fading (also called as the small-scale fading [1]) had better be excluded from the choice of the active set. For example, the pilots in IS-95 are sent every 26.66ms for a spread rate of 1.2288Mcps [1] and there are enough fast fading samples to be averaged out in the choice of the active set [2]. Therefore, the selection of the active set had better be determined by the path loss with the slow varying shadowing effect. Second, in practical CDMA systems (For example, IS-95), the MS can easily estimate the time delay, the phase and magnitude of the multipath components to find the stronger signal components [1]. This is because the pilot channel signal level is 4 to 6 dB higher than the traffic channel and the interference mainly comes from pilot channels from surrounding BSs. Third, the usage of T_{TDROP} timer to model the duration of BSs in the active set can be ignored in the system level design. T_{TDROP} is useful to account for the the correlation between signals in adjacent locations (or time interval) and avoids unnecessary handoff traffic. However, in system level design, the area taken into consideration is large enough and in the order of 10m. Therefore, the fadings between different location areas are independent [1]. Finally, the estimation of the pilot signal strength in term of path loss with shadowing is as easy as the estimation of energy-per-chip-to-interference. Lognormal distributed large-scale shadowing path loss model [1] is more appropriate to select BS into the active set.

This approach is established as follows: First, if we assume that the fraction of BS power allocated from different BSs to MS are the same in the forward link of a power-controlled system, we can use normalized path loss to define reference BS_0 as the one having the smallest path loss as shown in Fig. 2.2. Second, if the path loss of a BS exceeds that of the reference BS_0 by less than Th dB, that BS is put in

[1] chip per second

[2] The fast fading samples have correlation coefficients greater than zero for a duration of about 4ms at doppler shift of 100Hz [1]

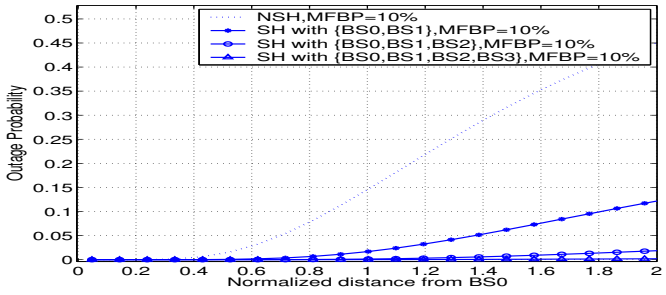

Figure 2.2. Soft handoff model using relative pilot strengths.

the active set (or in soft handoff with the MS). If the path loss of a BS exceeds that of the reference BS_0 by greater than Th dB, that BS is not in the active set (or in non-soft handoff with the MS). Third, if other BS has path loss less than the current reference BS_0, the reference BS is changed to that BS. The MS always connects to the BSs in the active set and the active set always includes the reference BS.

The definition of reference BS has its meanings in the reverse link. Because the reference BS has the lowest path loss [3] and due to the symmetric of propagation [1], the signal received at the reference BS from the MS is the strongest and more likely has a lower average frame error rate (FER) [4]. The reverse link uses the select combination to select the BS having the smallest FER [1] to power-control the MS and thereby, the reference BS is more likely to be the power-control BS for the MS in the reverse link.

[3]The path loss is the mean (local mean or time average) path loss and takes into account of the large-scale lognormal shadowing, which is the shadowing effects due to blocking between the transmitter and the receiver

[4]FER is determined by the signal-to-interference ratio at the BS. However, the interference level can be assumed to be the same if assuming all BSs are equally loaded and the MSs is uniformly distributed in every cell.

2.3.2 This is an example of a very long section title. It should appear single-spaced in the table of contents and not extend all the way to the page numbers. Look in the file chap1.tex to see how this is done.

Symmetric correlated lognormal shadowing model is a simple but effective approach to study the correlation between received signals from different BSs. This model was adopted widely [1]. The path loss l_i from BS_i to the MS is assumed to follow a lognormal distribution and is expressed as $l_i = r_i^u 10^{x_i/10}$, where r_i is normalized distance from BS_i to the MS (normalized to the radius of the cell), u is path loss slope and x_i is a Gaussian random variable with zero mean and σ standard deviation. Usually, the path loss can be expressed in dB as

$$L_i = 10\log_{10} l_i = 10\log_{10}(r_i^u 10^{x_i/10}) = M_i + a\xi + b\xi_i \tag{2.1}$$

where $M_i = 10u\log_{10}(r_i)$ and x_i is expressed as the weighed summation of two independent Gaussian random variables ξ and ξ_i with identical zero mean and σ standard deviation to account for correlation effects. Signals from different BSs are assumed to have the same correlation coefficient of $E[x_i x_j]/\sigma^2 = a^2$, $i \neq j$ if we limit $a^2 + b^2 = 1$.

2.3.3 Soft handoff and Non-soft Handoff Probability

Assume the active set is $N_{set} = \{0, i_1, i_2, ..., i_M\}, i_k \in \{1, 2, \ldots, N\}$, where N is the total number of BSs taken into consideration (refer to Fig. 2.1, N is 13 in our cells cluster structure). Following the definition of the SH and NSH in section 2.3.1, the probability of SH with active set N_{set} is derived as

$$\begin{aligned} P\{NSH\} =& P\{L_0 + Th < L_i, i = 1, 2, \cdots, N\} \\ =& E_z[\prod_{i=1}^{N} Q(z + c_i)] \end{aligned} \tag{2.2}$$

CHAPTER 3

SYSTEM DESCRIPTION

3.1 Introduction

The problem of evaluating the error rate performance of digital coherently detected systems in the presence of AWGN and carrier phase error (usually called partially coherent detection) is being well known and extensively studied in the literature [1]-[8]. Due to their bandwidth efficiency and good error rate performance, BPSK and QPSK are the most investigated systems. In the early studies [1], [2], and [3], the BEP of partially coherent PSK systems was obtained by numerically integrating the conditional BEP expression for a fixed phase error over the phase error statistic. Later on, many authors [4],[5],[6],[7] and [8] have approached this problem by either deriving upper and lower bounds (e.g. Chernoff and Jensen bounds) or by using infinite series approximations (e.g. Fourier and Maclaurin series) to evaluate the average BEP of such systems.

The aforementioned studies did not take channel fading into account.

And such extension is first targeted by [9], but provided only limited detailed results on that. Most recently, the authors in [10] used Maclaurin series to obtain accurate approximation for the average BEP of partially coherent BPSK and QPSK for several channel fading models, but large tracking-loop SNR was assumed in their analysis. For analytical purposes, it is desirable to have a good approximation, or a tight bound with less restrict assumptions on the system.

Table 3.1. Base Class 1 System Frequecies

Band	Reverse Link (MHz)	Forward Link (MHz)
A	1850-1865	1930-1945
D	1865-1870	1945-1950
B	1870-1885	1950-1965
E	1885-1890	1965-1970
F	1890-1895	1970-1975
F	1895-1910	1975-1990

In next section, such lower bound on the error rate performance of partially coherent BPSK and QPSK Nakagami-m fading systems using the Jensen's inequality is obtained. In this letter, we basically extend the work done by Najib and Prabhu [5] by considering channel fading impairment in the analysis. Section 3 presents some numerical results while our conclusion is in section 4.

3.2 Bounds Derivation

In this section we will use the Jensen's inequality as in [5] to derive lower bounds on the error probabilities of BPSK and QPSK Nakagami-m faded systems under imperfect carrier phase recovery condition.

3.2.1 BPSK Case

The BEP of BPSK in the presence of AWGN and for a given channel fading magnitude and carrier phase error can be written as [4]

$$P_2(e|\alpha,\epsilon) = \frac{1}{2}\,\mathrm{erfc}\left(\sqrt{\gamma}_b\ \alpha\ \cos\epsilon\right), \tag{3.1}$$

where E_b/N_0 is the average signal-to-noise (SNR) per bit. α is the magnitude of the channel fading gain. Here, we assumed a slowly Nakagami-m faded channel, hence, α (as well as ϵ) would remain constant over the data symbol duration T with probability density function (pdf) given as

$$p\ (\alpha) = \frac{2m^m}{\Omega^m \Gamma(m)}\ \alpha^{2m-1} e^{-\frac{m}{\Omega}\ \alpha^2}, \quad \alpha \geq 0 \tag{3.2}$$

where $\Omega = E[\alpha^2]$ is the envelope average power, $\Gamma(.)$ in the Gamma function, and $m \geq 0.5$ is the fading severity parameter. The Nakagami-m distribution spans many fading distributions. For $m = 0.5$ it becomes one-sided Gaussian distribution, for $m = 1$ it becomes Rayleigh distribution, and no fading case is obtained when $m \to \infty$.

The phase reference error ϵ is typically modeled by Tikhonov distribution that given by [2]

$$p\ (\epsilon) = \frac{e^{\rho_c \cos\epsilon}}{2\pi I_0(\rho_c)}, \quad |\epsilon| \leq 0 \tag{3.3}$$

this distribution is applied when the carrier phase is derived from unmodulated carrier tone using a first-order phase-locked loop, as well as, a second order PLL when the SNR in the loop bandwidth ρ_c is large [2]. In most practical interest, $\rho_c >> 1$, in which case the rms phase error $\sigma_\epsilon \simeq \rho_c^{-1/2}$. However, exact relationship between σ_ϵ and ρ_c is given in [2] . $I_n(.)$is the nth order modified Bessel function of the first kind.

The Jensen's inequality states that for any real-valued convex function $\xi(x)$ in a finite-mean random variable x , the mean of $\xi(x)$ is lower bounded by the function value at the mean of x [2] . Mathematically,

$$E\left[\xi(x)\right] \geq \xi\left(E[x]\right), \tag{3.4}$$

where $E[.]$ is the mathematical expectation. Since the error function in (3.1) is not a convex function in over the entire domain of ϵ , the Jensen inequality is not applicable

to it. Instead by using the simple inequality $\cos x \leq |\cos x|$, a lower bound of (3.1) can be written as

$$P_2(e|\alpha,\epsilon) \geq \frac{1}{2}\ \mathrm{erfc}\left(\sqrt{\gamma_b\ \cos^2\epsilon}\ \alpha\right), \tag{3.5}$$

It can be readily shown that the right hand side of (3.5) is now a convex function in $\cos^2\epsilon$ for all $|\epsilon| \leq \pi$. By applying Jensen's inequality to (3.5) the BEP of BPSK under given is lower bounded by

$$P_2(e|\alpha) = E\left[P_2(e|\alpha,\epsilon)\right]|_\epsilon \geq \frac{1}{2}\ \mathrm{erfc}\left(\sqrt{\gamma_b\ L_2}\ \alpha\right), \tag{3.6}$$

where $L_2 = E[\cos^2\epsilon]$ is the average power loss in the BPSK signal due to ϵ . For the distribution given in (3.3), one can write

$$L_2 = \frac{1}{2\pi I_0(\rho_c)} \int_{-\pi}^{\pi} e^{\rho_c \cos x} \cos^2 x\ dx = \frac{1}{2}\left[1 + \frac{I_2(\rho_c)}{I_0(\rho_c)}\right]. \tag{3.7}$$

To eliminate the dependence of (3.6) on α we have to average it over all values of α . That is

$$P_2(e) \geq\ \frac{1}{2}\int_0^{\infty} \mathrm{erfc}\left(\sqrt{\gamma_b\ L_2}\ \alpha\right) p\ (\alpha)\ d\alpha. \tag{3.8}$$

For the distribution given in (3.2), a closed form solution of (3.8) can be written using [11, eq. 6.286.1] as

$$P_2(e) \geq\ \frac{m^{m-1}\Gamma(m+1/2)}{2\Omega^m\sqrt{\pi}\ \Gamma(m)\left(\gamma_b L_2\right)^m}\ F\left(m, m+1/2; m+1; -\frac{m}{\Omega\gamma_b L_2}\right), \tag{3.9}$$

where $F(a,b;c;x)$ is the Gaussian hypergeometric function.

3.2.2 QPSK Case

The derivation of BEP in the QPSK case will be based on the assumption that the pair of information bits is mapped into the four phases using the Gray-encoding

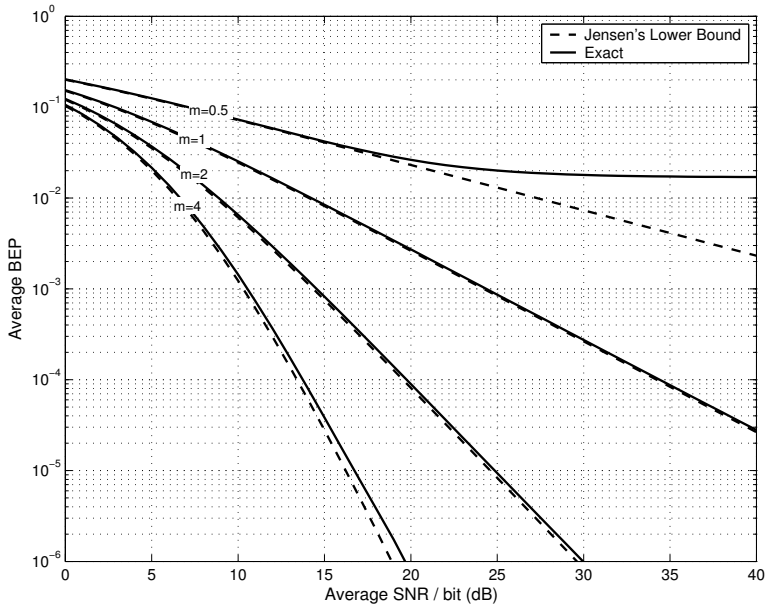

Figure 3.1. Average bit error probability of partially coherent Nakagami-m BPSK channel, $\sigma_\epsilon = 16^o$.

scheme in which the adjacent assigned bits differ only in one position. According to that, the BEP conditioned on α and ϵ and assuming equally probable symbols can be shown to be [4]

$$P_2(e|\alpha,\epsilon) = \frac{1}{4}\,\mathrm{erfc}\left(\sqrt{2\gamma_b}\;\alpha\;\cos(\epsilon+\pi/4)\right) + \frac{1}{4}\,\mathrm{erfc}\left(\sqrt{2\gamma_b}\;\alpha\;\cos(\epsilon-\pi/4)\right), \quad (3.10)$$

using $2\cos^2(x \mp \pi/4) = 1 \pm \sin 2x$, the right hand side of (3.10) can be bounded by

$$\begin{aligned} P_2(e|\alpha,\epsilon) \geq\; & \frac{1}{4}\,\mathrm{erfc}\left(\sqrt{\gamma_b(1+\sin 2\epsilon)}\;\alpha\right) + \frac{1}{4}\,\mathrm{erfc}\left(\sqrt{\gamma_b(1-\sin 2\epsilon)}\;\alpha\right) \\ =\; & \frac{1}{4}\,\mathrm{erfc}\left(\sqrt{\gamma_b(1+|\sin 2\epsilon|)}\;\alpha\right) + \frac{1}{4}\,\mathrm{erfc}\left(\sqrt{\gamma_b(1-|\sin 2\epsilon|)}\;\alpha\right). \end{aligned} \quad (3.11)$$

Noting that $P_4(e|\alpha,\epsilon)$is a convex function in $|\sin 2\epsilon|$. So, the average of $P_4(e|\alpha,\epsilon)$ over ϵ in the last equation can be further bounded by

$$P_2(e|\alpha) \geq\; \frac{1}{4}\,\mathrm{erfc}\left(\sqrt{\gamma_b\;L_4^+}\;\alpha\right) + \frac{1}{4}\,\mathrm{erfc}\left(\sqrt{\gamma_b\;L_4^-}\;\alpha\right), \quad (3.12)$$

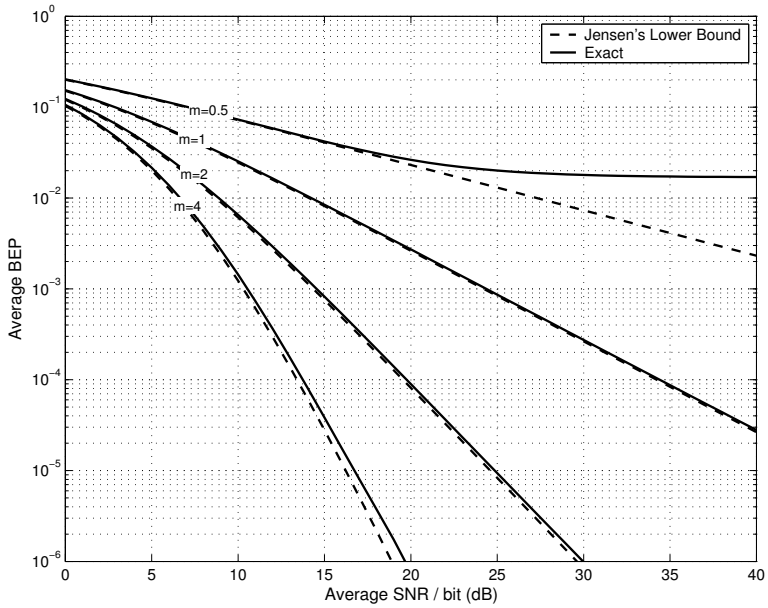

Figure 3.2. Average bit error probability of partially coherent Nakagami-m BPSK channel, $\sigma_\epsilon = 12^o$.

where $L_4^+ = E\left[1 + |\sin 2\epsilon|\right]$ and $L_4^- = E\left[1 - |\sin 2\epsilon|\right]$ are the average power losses in the QPSK quadrature carriers. Again for Tikhonov phase error distribution ϵ , it was shown that [5]

$$L_4^+ = 2 - L_4^- = 1 + \frac{4}{\pi \rho_c^2 I_0(\rho_c)} \left[\rho_c \sinh \rho_c - \cosh \rho_c + 1\right]. \tag{3.13}$$

Finally, by integrating (3.12) over the pdf of α, the average BEP of QPSK system under investigation is lower bounded by

$$P_2(e) \geq \frac{m^{m-1}\Gamma(m+1/2)}{4\Omega^m \sqrt{\pi}\ \Gamma(m)} \left[\vartheta(m, \gamma_b, L_4^+) + \vartheta(m, \gamma_b, L_4^-)\right], \tag{3.14}$$

where

$$\vartheta(a, b, c) = \frac{F\left(a, a+1/2; a+1; -\frac{a}{\Omega bc}\right)}{(bc)^a}. \tag{3.15}$$

To summarize, a lower bound for the average BEP of partially coherent Nakagami-m faded BPSK system is given in (3.9) and (3.7) and for QPSK system in (3.14)

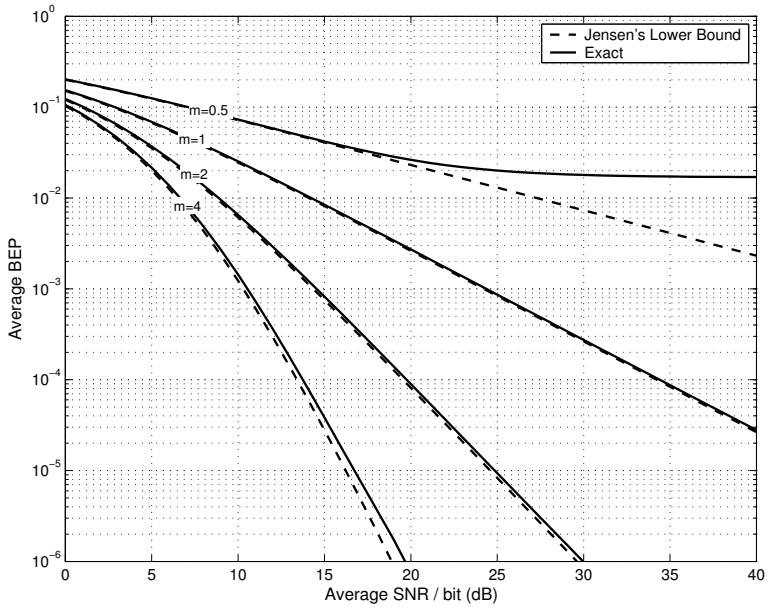

Figure 3.3. Average bit error probability of partially coherent Nakagami-m QPSK channel, $\sigma_\epsilon = 10^o$.

together with (3.13) and (3.15). The question is how to evaluate the Gaussian hypergeometric function $F(m, m + 1/2; m + 1; x)$that appears in the bounds expressions. This is what we will investigate in the next paragraphs.

3.2.3 Special Cases

3.2.3.1 For one-sided Gaussian fading (m=1/2)

For m=1/2 and by using [12, eq. 15.1.5]

$$F(1/2, 1; 3/2; -x^2) = x^{-1} \tan^{-1} x. \tag{3.16}$$

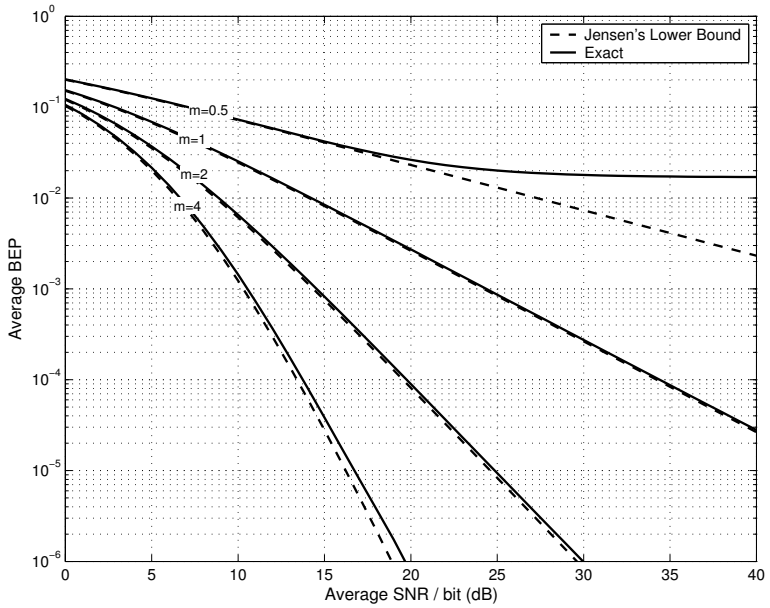

Figure 3.4. Average bit error probability of partially coherent Nakagami-m QPSK channel, $\sigma_\epsilon = 6^o$.

3.2.3.2 For integer m

If m is integer, a recursive down formula[12, eq. 15.2.12] can be used to evaluate $F(m, m + 1/2; m + 1; x)$ as

$$F(a, b; v - 1; x) = c_1(a, b, v, x)F(a, b; v; x) + c_2(a, b, v, x)F(a, b; v + 1; x), \qquad (3.17)$$

where

$$\begin{aligned} c_1(a, b, v, x) &= \frac{v[v - 1 - (2v - a - b - 1)x]}{v(v - 1)(1 - x)} \\ c_2(a, b, v, x) &= \frac{(v - a)(v - b)x}{v(v - 1)(1 - x)}. \end{aligned} \qquad (3.18)$$

Let $a = m, b = m + 1/2$, and $v = 2m$ and keep calculating till $v = m + 2$ .The seed values to start with can be calculated from [12, eq's. 15.1.13,14] as

$$\begin{aligned} F(m, m + 0.5; 2m + 1; x) &= 2^{2m} \left[1 + (1 - x)^{1/2}\right]^{-2m} \\ F(m, m + 0.5; 2m; x) &= 2^{2m-1}(1 - x)^{-1/2} \left[1 + (1 - x)^{1/2}\right]^{1-2m}. \end{aligned} \qquad (3.19)$$

Note that for the Rayleigh fading case where m=1, $F(m, m+1/2; m+1; x)$ can be evaluated directly from (3.19).That is,

$$F(1, 3/2; 2; x) = 2(1-x)^{-1/2}\left[1+(1-x)^{1/2}\right]^{-1}. \tag{3.20}$$

3.3 Results

The bound for BPSK system as given in (3.9) is plotted in Fig. 1 for different fading parameter m as a function of SNR at rms phase error of $\sigma_\epsilon = 16^o$ and in Fig. 2 at $\sigma_\epsilon = 12^o$. Similar results for the QPSK case using (3.14) and (3.15) are presented in Fig. 3 at $\sigma_\epsilon = 10^o$ and in Fig. 4 at $\sigma_\epsilon = 6^o$. Exact results using Fourier series approximation as derived in [13] are also shown for validation purposes.

From these figures one can note that the tightness of these bounds increases as the tracking loop SNR increases (i.e. the rms phase error σ_ϵ decreases). In the BPSK case, the bound leads to the exact result at $\sigma_\epsilon \leq 12^o$, while the bound reaches to the exact results at $\sigma_\epsilon \leq 5^o$ in the QPSK case. We expect that since the QPSK requires much higher degrees of phase precision than the BPSK case. This is due to the cross-talk interference between the QPSK quadrature carriers that introduced by the carrier phase error. Even for higher rms phase error, the degradation in the error performance between the derived bounds and the exact results is about 0.3 dB in the BPSK case at a BEP of 10^{-4} and m=4, and about 1 dB in the QPSK case at a BEP of 10^{-4} and m=2. These values corresponding to $\sigma_\epsilon = 16^o$ in BPSK case and $\sigma_\epsilon = 10^o$ in QPSK case.

Also, the figures clearly show that the tightness of the bounds is better for deeply faded environment (i.e. small m) than for less sever fading environment. This

can be explained as follow. The bounds were derived for the phase error loss terms ($\cos\epsilon$ in the BPSK case and $1 \pm sin2\epsilon$ in the QPSK case), while exact analysis of the fading effect was done. That means in deeply fading environment where the system performance is dominated by fading rather than the phase error, the bounds will be much tightness. Anyway, for most practical cases, the bounds remain tight enough to be useful as a design tool.

3.4 Conclusions

Lower bounds on the error probability of Nakagami-m faded BPSK and QPSK channels operating in a noisy carrier synchronization environment have been derived. The derivation is based on the Jensen's inequality of defined convex functions. These bounds were shown to be tight for practical range of the rms phase errors. that, and equally important, is the simplicity of the solution approach afforded by those bounds compared to the series approach solution given in [13], or [10].

APPENDIX A

JENSEN'S INEQUALITY FOR CONVEX FUNCTIONS

In this appendix, we present a procedure for improving the bounds obtained by the application of Jensen's inequality. The methiod is based on the idea of reducing the thickness of a convex region into many thinner convex regions.

A.1 Convex Functions

A real valued function f is defined to be convex over an interval $\Omega = [\alpha, \beta]$ if

$$\lambda\Phi\{x_1) + (1-\lambda)\Phi(x_2) \geq \Phi(\lambda x_1 + (1-\lambda)x_2\}. \tag{A.1}$$

If the above inequality is reversed or

$$\lambda\Phi(x_1) + (1-\lambda)\Phi(x_2) \leq \Phi(\lambda x_1 + (1-\lambda)x_2), \tag{A.2}$$

then Φ is called concave.

A.2 Jensen's Inequality for Convex Functions

Let x be a random variable with a finite mean. If $\Phi(x)$ is real-valued convex function, then

$$E[\Phi(x)] \geq \Phi\left(E[x]\right) \tag{A.3}$$

where $E[.]$ is the mathematical expectation.

APPENDIX B

UPPER BOUNDS ON MOMENTS

In this appendix, we compute upper bounds on the moments of random variables.

B.1 Computation of Bounds

Note that

$$\cos(x) \leq 1 - \frac{2}{\pi^2}x^2, \quad |x| \leq \pi \tag{B.1}$$

and

$$\cos(x) \geq 1 - x^2, \quad |x| \leq \pi. \tag{B.2}$$

REFERENCES

[1] W. B. M. Schwartz and S. Stein, *Communication Systems and Techniques.* New York, NY: McGraw-Hill, 1966.

[2] A. Viterbi, *Principles of Coherent Communication.* New York, NY: McGraw-Hill, 1966.

[3] W. Lindsey and M. Simon, *Telecommunication Systems Enginnering.* Upper Saddle River, NJ: Prentice Hall, 1973.

[4] V. Prabhu, "Psk performance with imperfect carrier phase recovery," *IEEE Trans. Aerosp. Electron. Syst.*, vol. ASE-12, pp. 275–286, Mar. 1976.

[5] M. Najib and V. Prabhu, "Lower bounds on error performance for bpsk and qpsk systems with imperfect carrier phase recovery," in *Proc. IEEE Int. Conf. Commun. Technology*, Atlanta,GA, June 1998, pp. 1253–1258.

[6] G. Kaplan and U. Ram, "Bounds on performance for noisy reference psk channel," *IEEE Trans. Commun.*, vol. COM-38, pp. 1699–1707, Oct. 1990.

[7] K. S. P. Kam, S. Teo and T. Tjhung, "Approximate results for the bit error probability of binary phase shift keying with noisy phase reference," *IEEE Trans. Commun.*, vol. COM-341, pp. 1020–1022, July 1993.

[8] Y. Some and P. Kam, "Bit-error probability of qpsk with noisy phase reference," *IEE-Proc.-Commun.*, vol. 142, pp. 292–296, Oct. 1995.

[9] W. Weber, "Performance of phase-locked loops in the presence of fading communication channels," *IEEE Trans. Commun.*, vol. COM-24, pp. 487–499, May 1976.

[10] M. Simon and M. Alouini, "Simplified noisy reference loss evaluation for digital communication in the presence of slow fading and carrier phase recovery," *IEEE Trans. Veh. Technol.*, vol. 50, pp. 783–791, Mar. 2001.

[11] I. Gradeshteyn and I. Ryzhik, *Table of Integrals, Series, and Products.* New York, NY: Academic, 1994.

[12] M. Abramowitz and I. Stegun, *Handbook of Mathematical Functions.* NY: Dover, 1972.

[13] M. Smadi and V. Prabhu, "Performance analysis of partially coherent psk systems in wireless channels with equal gain diversity receivers," *Proc. IEE, Communications*, submitted for publication.

BIOGRAPHICAL STATEMENT

Jay V. Smith was born in Atteel, Palestine, in 1965. He received his B.S. degree from Baghdad University, Iraq, in 1988, his M.S. and Ph.D. degrees from The University of Texas at Arlington in 1993 and 1999, respectively, all in Electrical Engineering. From 1988 to 1991, he was with the department of Electrical Engineering, Baghdad University as an Instructor in the Communications and Electronics Labs. In 1995, he joined Nortel Networks, Wireless Engineering Networks as RF engineer then as a technical advisor for the design and optimization of CDMA mobile and fixed wireless access systems. His current research interest is in the area of CDMA communications for mobile cellular systems. He is a member of several IEEE societies.